COUPLED-INDUCTOR CURRENT-DOUBLER TOPOLOGY IN PHASE-SHIFTED FULL-BRIDGE DC-DC CONVERTER

A. Pietkiewicz and D. Tollik
Ascom Energy Systems
Belpstrasse 37, CH – 3000 Berne 14, Switzerland
Phone: + 41 31 9994384   Fax: + 41 31 9994236

Abstract – The paper proposes and analyses the coupled-inductor version of the current-doubler rectifier. The analysis shows that coupling of the inductors can reduce losses both in transformer and inductor windings. Practical design procedure of the coupled-inductor and experimental results for 1900 W telecom rectifier are included.

1. INTRODUCTION

Current-doubler topology was presented in the literature as a possible way to reduce power losses in the transformer secondary side winding of the full-wave buck-derived converters, such as push-pull, half-bridge [1], [2] and full-bridge [3], [4]. In comparison to conventional center-tapped topology these losses can be decreased by approx. 50%. The penalty for that improvement is a need for an additional inductor. This inconvenience can be partially alleviated by integrating both inductors on a common core. Integration without magnetic coupling of the windings was discussed in [1] and [4].

The main goal of this paper is to propose and analyse current-doubler with coupled-inductor and to show its advantages over the non-coupled version.

The electrical schematic and inductor winding arrangement for the coupled-inductor version of the current-doubler are shown in Fig. 1.

Section 2 of the paper shows the proposed coupled-inductor and derives its electrical model needed for further analyses. Section 3 presents derivation of analytical expressions for current waveforms in the coupled-inductor current doubler and discusses influence of the coupling coefficient on these waveforms. Section 4 shows that the coupling of windings reduces rms current values in the transformer secondary and inductor windings. In Section 5 the flux waveforms in the core are derived to determine its saturation conditions. Section 6 presents practical design procedure of the coupled-inductor and some experimental results on 1900 W telecom rectifier. Section 7 summarises the most interesting conclusions of the paper.

2. COUPLED - INDUCTOR AND ITS MODEL

In this section the proposed coupled-inductor structure will be presented, parameters of its reluctance and electrical models will be derived and their relationships discussed.
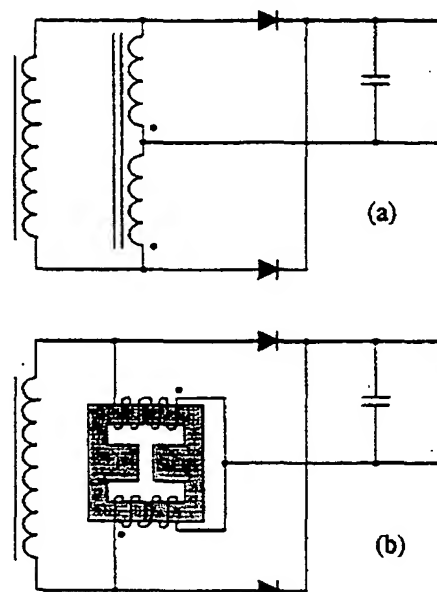

Fig. 1. The proposed coupled-inductor current-doubler: (a) electrical schematic, (b) coupled-inductor realisation.

The proposed coupled-inductor structure is shown in Fig. 2. The windings are placed on the outer legs of the double E-type core. Direction of the windings is so that the fluxes produced by the currents i_1 and i_2 add together in the center leg. Both windings have the same number of turns equal N.
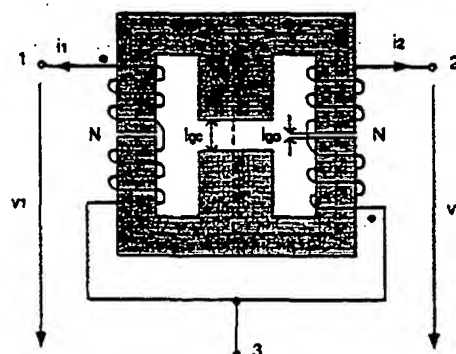

Fig. 2. Realisation of the coupled-inductor.

The core has air-gap l_{gc} in the center leg and two equal air-gaps l_{go} in the two outer legs. Simplified reluctance model of such magnetic structure is shown in Fig. 3.
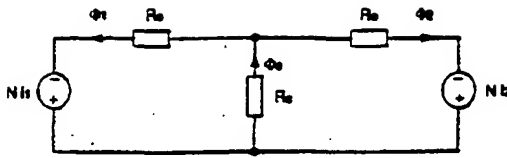
Fig. 3. Reluctance model of the coupled-inductor.

In the above model R_o represents the reluctance of each outer core leg, which is normally dominated by the reluctance of the air-gap. R_c represents the equivalent reluctance of the center leg, which consists of two components, one resulting from the air-gap l_{gc} and the other one from the stray field. In practice the stray field component can quite strongly influence the value of R_c, which makes calculation of the required air-gap very difficult.

The model of Fig. 3 can be easily described by the following equations:

$$\Phi_1 = \frac{R_c + R_o}{R_o \cdot (R_o + 2 \cdot R_c)} \cdot N \cdot i_1 - \frac{R_c}{R_o \cdot (R_o + 2 \cdot R_c)} \cdot N \cdot i_2 \quad (1a)$$

$$\Phi_2 = \frac{R_c}{R_o \cdot (R_o + 2 \cdot R_c)} \cdot N \cdot i_1 + \frac{R_c + R_o}{R_o \cdot (R_o + 2 \cdot R_c)} \cdot N \cdot i_2 \quad (1b)$$

Multiplying (1) by N and then differentiating with respect to time gives:

$$v_1 = N \cdot \frac{d\Phi_1}{dt} = L_o \cdot \frac{di_1}{dt} - M \cdot \frac{di_2}{dt} \quad (2a)$$

$$v_2 = N \cdot \frac{d\Phi_2}{dt} = -M \cdot \frac{di_1}{dt} + L_o \cdot \frac{di_2}{dt} \quad (2b)$$

where:

$$L_o = N^2 \cdot \frac{R_c + R_o}{R_o \cdot (R_o + 2 \cdot R_c)} \quad (3a)$$

$$M = N^2 \cdot \frac{R_c}{R_o \cdot (R_o + 2 \cdot R_c)} \quad (3b)$$

Manipulating eqs. (2) one can obtain:

$$v_1 = (L_o - M) \cdot \frac{di_1}{dt} - M \cdot (\frac{di_2}{dt} - \frac{di_1}{dt}) \quad (4a)$$

$$v_2 = -M \cdot (\frac{di_1}{dt} - \frac{di_2}{dt}) + (L_o - M) \cdot \frac{di_2}{dt} \quad (4b)$$

Now eqs. (4) can be represented in the circuit model form shown in Fig. 4. The model is composed of the ideal transformer with 1 : 1 turns ratio, the mutual inductance M and the inductance L, which is equal:

$$L = L_o - M \quad (5)$$

Combining (3) and (5) yields:
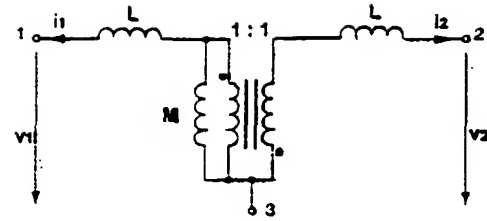
$$L = \frac{N^2}{R_o + 2 \cdot R_c} \quad (6a)$$

Fig. 4. Electrical model of the coupled-inductor.

$$M = \frac{R_c}{R_o} \cdot L \quad (6b)$$

In addition to L and M in the further analysis the coupling coefficient k defined as:

$$k = \frac{M}{\sqrt{L_o \cdot L_o}} = \frac{M}{L + M} \quad (7a)$$

will be used. Inserting now (6) in (7a) the coupling coefficient k can be expressed by the parameters of th reluctance model:

$$k = \frac{1}{1 + \frac{R_o}{R_c}} \quad (7b)$$

Eqs. (6) and (7b) link parameters of the electrical model of Fig. 4 with the elements of the reluctance model of Fig. 3.

The analytical relation between parameters of the reluctance model and physical parameters of the core is difficult to establish and in practice size of the air-gaps must be selected experimentally. The reluctance model facilitates however understanding of the influence of the air-gaps on the parameters of the electrical model from Fig. 4. For example, it enables to note that changing the proportion l_{go} to l_{gc} one can influence proportion R_o to R_c and thus modify the values of the mutual inductance M and coupling coefficient k. For $R_o \gg R_c$ (air-gaps in the outer legs only) the inductance M and coupling coefficient k are close to 0 while for $R_o \ll R_c$ (air-gap in the center leg only) the inductance M becomes much larger than L and k approaches 1. Keeping additionally the sum of $R_o + 2 \cdot R_c$ constant, one can change M and k without influencing the value of the inductance L (see eq. 6a). In this way the influence of the coupling coefficient on the current-doubler parameters can be conveniently analysed without affecting the value of inductance L.

3. CURRENT WAVEFORMS IN THE COUPLED-INDUCTOR CURRENT-DOUBLER

The goal of this section is to derive analytical expressions for the current waveforms of the coupled-inductor current-doubler and to analyse the influence of the coupling coefficient k.

Current waveforms

To derive the current waveforms, the electrical model of the coupled-inductor from Fig. 4 will be implemented in

the current-doubler circuit of Fig. 1. Then four intervals of the switching period will be discussed.

The current waveforms of the coupled-inductors i_1 and i_2 are composed of four linear sections each corresponding to one interval of the circuit operation. The current waveform in each interval will be described by two quantities, the increment Δi and the average value I. In Fig. 5 the examples of the waveforms i_1, i_2 and $i_1 + i_2$ are shown and their increments Δi as well as duty-ratio D and period T_s defined.
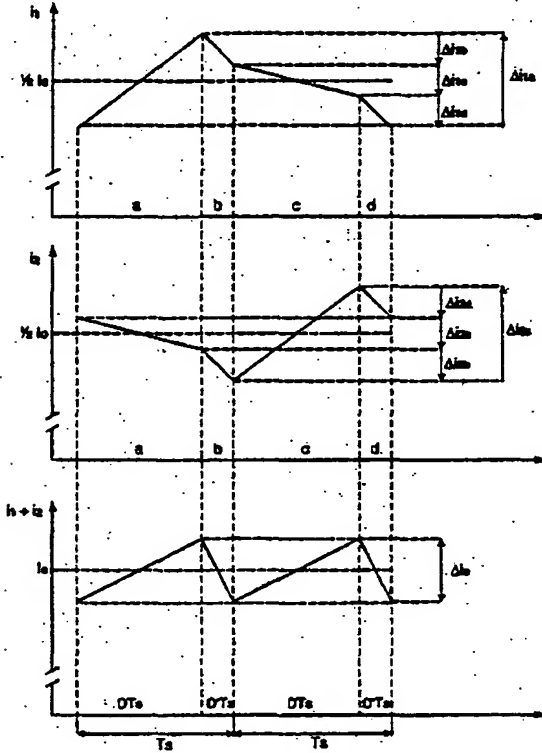

Fig. 5. Current waveforms in the coupled-inductor windings i_1, i_2 and their sum $i_1 + i_2$.

Interval "a":

The equivalent schematic for the first active interval "a" is presented in Fig. 6, where V_s is the voltage on the secondary winding of the transformer and V_o is the output voltage.
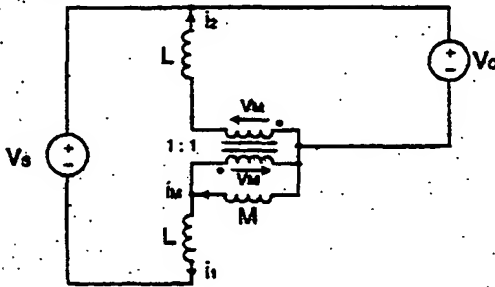

Fig. 6. Equivalent circuit for interval "a".

As seen from Fig. 6:

$$i_1 = i_M + i_2 \tag{8}$$

Differentiating with respect to time and multiplying by M yields:

$$M \cdot \frac{di_1}{dt} = M \cdot \frac{di_M}{dt} + M \cdot \frac{di_2}{dt} \tag{9}$$

Taking into account that:

$$M \cdot \frac{di_M}{dt} = v_M \tag{10}$$

and writing similar relations for the voltages on both inductances L one gets the following system of equations:

$$M \cdot \frac{di_1}{dt} - M \cdot \frac{di_2}{dt} = v_M \tag{11a}$$

$$L \cdot \frac{di_1}{dt} = V_s - V_o - v_M \tag{11b}$$

$$L \cdot \frac{di_2}{dt} = v_M - V_o \tag{11c}$$

Inserting (11b) and (11c) into (11a) and solving results in:

$$v_M = \frac{M}{L + 2 \cdot M} \cdot V_s \tag{12}$$

Using now (7a), eq. (12) can be rewritten as:

$$v_M = \frac{k}{1 + k} \cdot V_s \tag{13}$$

For the further derivations the expression for the output voltage V_o as a function of the voltage amplitude of the secondary winding V_s will be needed. Assuming that the dc voltage on each inductor winding is 0, V_o must be equal to the dc voltage value of each diode, for example D2. As seen from Figs. 6 through 9 this voltage is equal 0 during intervals "a", "b" and "d" and V_s during interval "c". Taking into account duration of the above intervals (refer to Fig. 5) it is easy to show that:

$$V_o = \frac{D \cdot V_s}{2} \tag{14}$$

Now substituting (13) and (14) into (11b) and (11c) leads to:

$$L \cdot \frac{di_1}{dt} = (2 - D - \frac{2 \cdot k}{1 + k}) \cdot \frac{V_o}{D} \tag{15a}$$

$$L \cdot \frac{di_2}{dt} = (\frac{2 \cdot k}{1 + k} - D) \cdot \frac{V_o}{D} \tag{15b}$$

Replacing dt with $D \cdot T_s$, di_1 with Δi_1 and di_2 with Δi_2 one can derive from (15a) and (15b) expressions for both current increments Δi_1 and Δi_2 and their sum $\Delta i_1 + \Delta i_2$ for the interval "a". The obtained results are presented in the Table 1.

The average current values of i_1 and i_2 during interval "a" are equal:

$$I_{1a} = I_{2a} = \frac{I_o}{2} \qquad (16)$$

where I_o is the output current.

Interval "b":

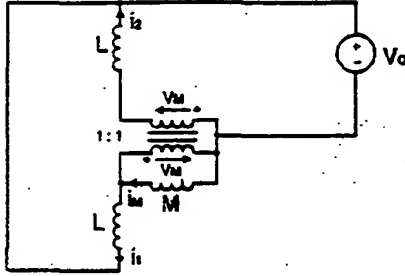The equivalent circuit for interval "b" is shown in Fig. 7.

Fig. 7. Equivalent circuit for interval "b".

Compared to Fig. 6 the only change is that the transformer secondary voltage V_s drops to 0 (passive interval) that can be used in (11b), (11c) and (12) to give:

$$L \cdot \frac{di_1}{dt} = -V_o \qquad (17a)$$

$$L \cdot \frac{di_2}{dt} = -V_o \qquad (17b)$$

Using similar procedure as above one obtains from (17) expressions for Δi_1, Δi_2 and $\Delta i_1 + \Delta i_2$ for this interval. The results are given in the Table 1.

The average current values for interval "b" can be found from the relations (refer to Fig. 5):

$$I_{1b} = I_{1a} + \frac{\Delta i_{1a}}{2} + \frac{\Delta i_{1b}}{2} \qquad (18a)$$

$$I_{2b} = I_{2a} + \frac{\Delta i_{2a}}{2} + \frac{\Delta i_{2b}}{2} \qquad (18b)$$

where Δi_{1a}, Δi_{1b}, Δi_{2a} and Δi_{2b} are given in the Table 1. The final results for I_{1b} and I_{2b} are shown in the Table 2.

Intervals "c" and "d":

The Figs. 8 and 9 show the equivalent circuits for the second active interval "c" and the second passive interval "d". Derivation of all current increments and average values for these intervals can be done in analogous way as it was shown above for intervals "a" and "b". All results are given in Tables 1 and 2.
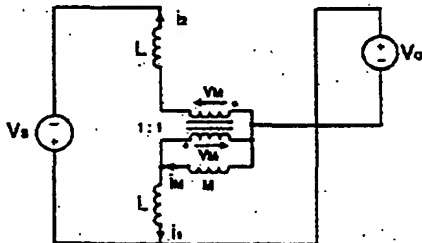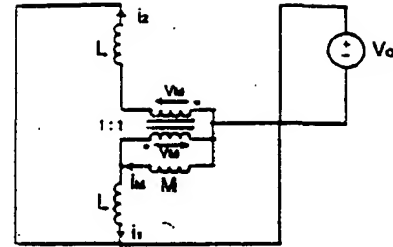

Fig. 8. Equivalent circuit for interval "c".

Fig. 9. Equivalent circuit for interval "d".

	Δi_1	Δi_2	$\Delta i_o = \Delta i_1 + \Delta i_2$
a	$\frac{T_s \cdot V_o}{L} \cdot (2 - D - \frac{2 \cdot k}{1 + k})$	$\frac{T_s \cdot V_o}{L} \cdot (\frac{2 \cdot k}{1 + k} - D)$	$\frac{2 \cdot T_s \cdot V_o}{L} \cdot (1 - D)$
b	$-\frac{T_s \cdot V_o}{L} \cdot (1 - D)$	$-\frac{T_s \cdot V_o}{L} \cdot (1 - D)$	$\frac{2 \cdot T_s \cdot V_o}{L} \cdot (1 - D)$
c	$\frac{T_s \cdot V_o}{L} \cdot (\frac{2 \cdot k}{1 + k} - D)$	$\frac{T_s \cdot V_o}{L} \cdot (2 - D - \frac{2 \cdot k}{1 + k})$	$\frac{2 \cdot T_s \cdot V_o}{L} \cdot (1 - D)$
d	$-\frac{T_s \cdot V_o}{L} \cdot (1 - D)$	$-\frac{T_s \cdot V_o}{L} \cdot (1 - D)$	$\frac{2 \cdot T_s \cdot V_o}{L} \cdot (1 - D)$

Table 1. Incremental components of the coupled-inductor currents in switching intervals "a" through "d".

	I_1	I_2	$I_1 + I_2$
a	$\frac{I_o}{2}$	$\frac{I_o}{2}$	I_o
b	$\frac{I_o}{2} + \frac{T_s \cdot V_o}{2 \cdot L} \cdot \frac{1 - k}{1 + k}$	$\frac{I_o}{2} - \frac{T_s \cdot V_o}{2 \cdot L} \cdot \frac{1 - k}{1 + k}$	I_o
c	$\frac{I_o}{2}$	$\frac{I_o}{2}$	I_o
d	$\frac{I_o}{2} - \frac{T_s \cdot V_o}{2 \cdot L} \cdot \frac{1 - k}{1 + k}$	$\frac{I_o}{2} + \frac{T_s \cdot V_o}{2 \cdot L} \cdot \frac{1 - k}{1 + k}$	I_o

Table 2. Average values of the coupled-inductor currents in switching intervals "a" through "d".

From the Tables 1 and 2 it can be concluded that:

- the coupling coefficient k influences current waveforms i_1 and i_2 but does not affect the output current $i_o = i_1 + i_2$

- current waveforms i_1 and i_2 are identical but shifted 180 degrees in phase.

To illustrate the influence of inductor coupling on the current waveforms Fig. 10 shows the example of the current i_1 for three values of the coupling coefficient k. It can be noted that when k approaches 1 both currents i_1 and i_2 become equal $\frac{1}{2} \cdot i_o$.
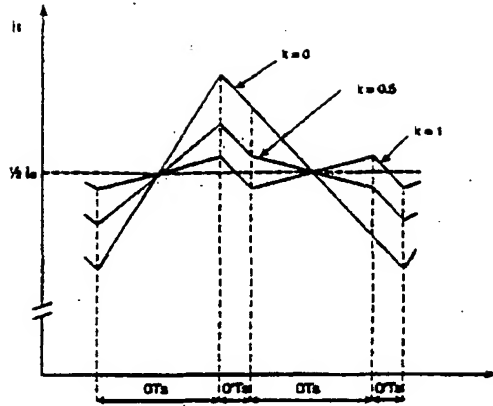
Fig. 10. Inductor current waveform i_1 for various coupling coefficient values k.

4. INFLUENCE OF THE INDUCTOR COUPLING ON THE RMS VALUES OF THE TRANSFORMER AND INDUCTOR CURRENTS

Transformer

The current waveform in the transformer secondary winding depends on the primary side converter topology. In this paper the phase-shifted full-bridge topology shown in Fig. 11 is considered.
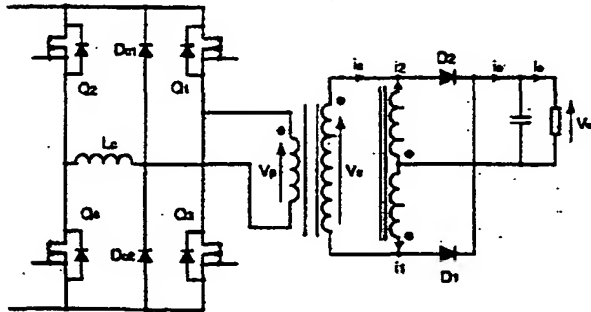

Fig. 11. Electrical schematic of the phase-shifted full-bridge with the coupled-inductor current-doubler.

Operation of the primary side has been discussed thoroughly in [5] and will not be repeated here. Particular feature of this topology is that for passive intervals "b" and "d" the current in the transformer secondary winding remains equal to the current of the coupled inductor i_1 and i_2, respectively. This results from the fact that the primary winding is shorted and the primary current maintains circulation through the commutating inductor L_c and some stray inductances of the transformer.

As a result the current waveform in the transformer secondary winding follows that of i_1 in intervals "a" and "b" and then changes direction and follows that of i_2 for the intervals "c" and "d". So to calculate the rms current values in the transformer secondary it is enough to consider only two intervals, for instant "a" and "b".

The derivation of the rms current value is based on the fact that for the piecewise linear waveforms composed of n intervals, each characterised by the duration τ_i, average value I_i and increment Δi_i, the following formula can be applied:

$$I_{rms}^2 = \sum_{i=1}^n \frac{\tau_i}{T_s} \cdot (I_i^2 + \frac{\Delta i_i^2}{12})$$ (19)

Thus the rms current value for transformer secondary $I_{s,rms}^2$ can be calculated from:

$$I_{s,rms}^2 = D \cdot (I_{1a}^2 + \frac{\Delta i_{1a}^2}{12}) + (1-D) \cdot (I_{1b}^2 + \frac{\Delta i_{1b}^2}{12})$$ (20)

Inserting now the relevant expressions from the Tables 1 and 2 and normalising to $0.5 \cdot I_o$ the formula for $(I_{s,rms} / 0.5 \cdot I_o)^2$ can be derived (not shown here for the sake of space). The calculated results for practical values $D = 0.8$ and $\Delta i_o = 0.2 \cdot I_o$ are shown in Fig. 12.
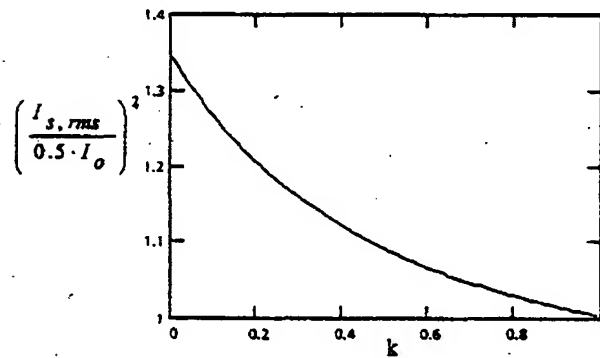

Fig. 12. Influence of the coupling coefficient k on rms current value in the transformer secondary winding.

The above curve shows that coupling of the inductors reduces the value of $(I_{s,rms}/0.5 \cdot I_o)^2$, and thus the copper losses in the transformer. This is a clear advantage of the coupled-inductor version over the non-coupled one.

In practical application forcing k very close to 1 is not recommended, as it does not bring much improvement in the losses and on the other hand, makes the inductor core sensitive to unsymmetry of the inductor dc currents (refer to Sec. 5).

Inductor

Each inductor winding has identical rms current value that can be calculated (for example for i_1) from:

$$I_{1,rms}^2 = 0.5 \cdot [D \cdot (I_{1a}^2 + \frac{\Delta i_{1a}^2}{12}) + (1-D) \cdot (I_{1b}^2 + \frac{\Delta i_{1b}^2}{12}) +$$

$$D \cdot (I_{1c}^2 + \frac{\Delta i_{1c}^2}{12}) + (1-D) \cdot (I_{1d}^2 + \frac{\Delta i_{1d}^2}{12})]$$ (21)

Similar procedure as described above leads to the formula for normalised rms current value of each inductor winding as a function of the coupling coefficient k. For duty-ratio $D = 0.8$ and output current ripple $\Delta i_o = 0.2 \cdot I_o$ the calculated results are presented in Fig. 13.
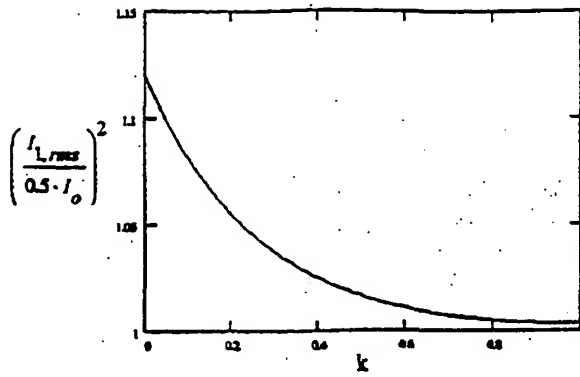
Fig. 13. Influence of the coupling coefficient k on rms current value in the coupled-inductor windings.

Also here it can be seen that coupling between the windings is desirable to reduce the rms current value and thus power losses in the coupled-inductor.

5. FLUX WAVEFORMS IN THE CORE OF THE COUPLED-INDUCTOR

Ac flux waveforms

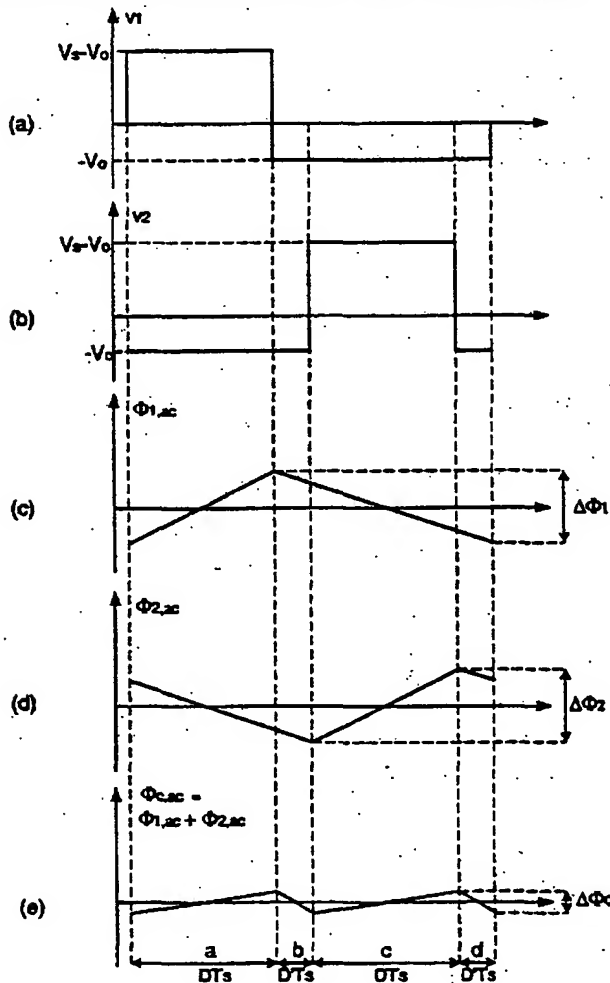Now the flux waveforms in the core of the coupled-

Fig. 14. Winding voltages and ac flux waveforms in the outer and center legs.

inductor will be derived. Similarly to the current waveforms the ac and dc components will be presented. To find ac flux components it is convenient to use voltage waveforms v_1 and v_2 on the two windings. These voltages are shown in Fig. 14 a and b.

Using the Faraday's formulas:

$$v_1 = N \cdot \frac{d\Phi_1}{dt} \tag{22a}$$

$$v_2 = N \cdot \frac{d\Phi_2}{dt} \tag{22b}$$

one can easy note that the ac components of the fluxes Φ_1 and Φ_2 have the waveforms shown in Fig. 14 c and d, where:

$$\Delta\Phi_1 = \Delta\Phi_2 = \frac{V_o \cdot T_s}{N} \cdot (2 - D) \tag{23}$$

It is worthwhile to note that the ac waveforms of Φ_1 and Φ_2 in contrary to current waveforms have only two linear segments during one period and do not depend on the coupling coefficient k.

The ac component of the flux in the center leg is shown in Fig. 14 e, where:

$$\Delta\Phi_c = \frac{2 \cdot V_o \cdot T_s}{N} \cdot (1 - D) \tag{24}$$

Notice that the ac flux waveform in the center leg has doubled frequency and smaller amplitude than the flux in the outer legs.

Dc flux waveforms

Dc flux components $\Phi_{1,dc}$ and $\Phi_{2,dc}$ and their sum $\Phi_{c,dc} = \Phi_{1,dc} + \Phi_{2,dc}$ can be obtained by combining eqs. (1), (3) and (5) for dc quantities:

$$\Phi_{1,dc} = \frac{L}{N} \cdot I_1 + \frac{M}{N} \cdot (I_1 - I_2) \tag{25a}$$

$$\Phi_{2,dc} = \frac{L}{N} \cdot I_2 + \frac{M}{N} \cdot (I_2 - I_1) \tag{25b}$$

$$\Phi_{c,dc} = \frac{L}{N} \cdot (I_1 + I_2) \tag{25c}$$

From (25) one can see that for M >> L (good coupling) the outer leg fluxes $\Phi_{1,dc}$ and $\Phi_{2,dc}$ are sensitive to dc current unsymmetry $|I_1 - I_2|$.

Since in the current-doubler topology there is no inherent mechanism forcing both windings to share equally the dc current it seems important to investigate factors influencing the possible current unsymmetry. This can be done using the dc model of the circuit shown in Fig. 15.

The resistors R_1, R_2 and R_s represent parasitic dc resistances f the inductor windings and transformer secondary, respectively. Th voltage sources V_{D1} and V_{D2} represent dc voltage components of both diodes D_1
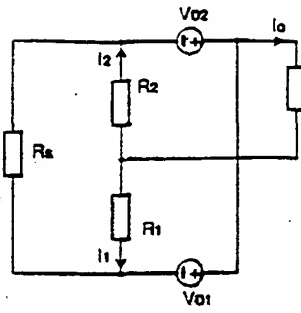
Fig. 15. Dc equivalent circuit of the current-doubler.

and D_2, respectively, and can be derived considering their voltage waveforms during all four switching intervals "a" through "d", as:

$$V_{D1} = \frac{1}{2} \cdot (D \cdot V_s - V_{F1} - V_{F2} - R_s \cdot I_1) \qquad (26a)$$

$$V_{D2} = \frac{1}{2} \cdot (D \cdot V_s - V_{F1} - V_{F2} - R_s \cdot I_2) \qquad (26b)$$

where V_{F1}, V_{F2} denote forward voltage drops of the corresponding diode. Solving the circuit of Fig. 15 one obtains the following expression for current unsymmetry:

$$\Delta I = I_1 - I_2 = I_o \cdot \frac{R_2 - R_1}{R_1 + R_2 + R_s} \qquad (27)$$

From (27) one can notice that the current unsymmetry can be caused by unequal resistances R_1 and R_2, while potential unequality of V_{F1} and V_{F2} is not relevant. Concluding it is important to pay attention to maintain total resistances R_1 and R_2 (including the corresponding layout traces) as equal as possible.

In practice, however the currents I_1 and I_2 are never identical. It affects the maximum flux value, that is derived in the following.

Denoting $I_1 = 0.5 \cdot (I_o + \Delta I)$ and $I_2 = 0.5 \cdot (I_o - \Delta I)$, inserting in (25) and manipulating one obtains:

$$\Phi_{1,dc} = \frac{L \cdot I_o}{2 \cdot N} \cdot (1 + \frac{2}{1-k} \cdot \frac{\Delta I}{I_o}) \qquad (28a)$$

$$\Phi_{2,dc} = \frac{L \cdot I_o}{2 \cdot N} \cdot (1 - \frac{2}{1-k} \cdot \frac{\Delta I}{I_o}) \qquad (28b)$$

It can now be easily seen that, assuming positive ΔI, $\Phi_{1,dc}$ is greater than $\Phi_{2,dc}$ and thus must be considered for the core saturation conditions.

Peak value of the flux

Adding to $\Phi_{1,dc}$ the half of the $\Delta \Phi_1$ from (23) the expression for maximum value of the total flux $\Phi_{1,max}$ is obtained:

$$\Phi_{1,max} = \frac{L \cdot I_o}{2 \cdot N} \cdot (1 + \frac{2}{1-k} \cdot \frac{\Delta I}{I_o} + \frac{2-D}{2 \cdot (1-D)} \cdot \frac{\Delta i_o}{I_o}) \qquad (29)$$

Eq. (29) describes the critical flux value that has to be taken into account during design process to avoid core saturation. It is interesting to notice that for k

approaching 1 $\Phi_{1,max}$ becomes quite sensitive to the dc current unsymmetry ΔI. This is a good reason to limit the value of k in practical design.

6. COUPLED-INDUCTOR DESIGN PROCEDURE AND EXPERIMENTAL RESULTS

Coupled-inductor design procedure

The following design procedure is proposed.

Step 1. Calculation of the inductance value L.

Assuming the ac component of the output current Δi_o, switching period T_s, output voltage V_o and duty-ratio D the inductance L can be calculated from the following equation, that can be derived from Table 1:

$$L = \frac{2 \cdot T_s \cdot V_o \cdot (1-D)}{\Delta i_o} \qquad (30)$$

Step 2. Determination of the coupling coefficient k.

The value of k is selected assuming the maximum anticipated current unsymmetry $\Delta I/I_o$ and its allowable influence on the value of $\Phi_{1,max}$ (see (29)).

Step 3. Selection of the core size.

Using the formula for the Area Product as derived in Appendix:

$$AP = \left[\frac{12 \cdot L \cdot I_o^2}{K_{Cu} \cdot B_{sat}} \cdot (1 + \frac{2}{1-k} \cdot \frac{\Delta I}{I_o} + \frac{2-D}{2 \cdot (1-D)} \cdot \frac{\Delta i_o}{I_o}) \right]^{1.31} \qquad (31)$$

where L should be inserted in H, B_{sat} in Tesla and I_o in Amps, the required AP in cm^4 and thus core size can be found.

Step 4. Determination of the turns number N.

Putting the AP value of the selected core into eq. (A4) from Appendix the value of maximum current density for 30 deg.C temperature rise J_{30} can be calculated. Then using (A3) the number of turns N is obtained.

Step 5. Selection of the air-gaps l_{go} and l_{ge}.

Since the calculation of the air-gaps is very difficult they must be selected experimentally. First knowing L and k one has to calculate the value of the inductance M:

$$M = \frac{k}{1-k} \cdot L \qquad (32)$$

Next selection of the air-gaps must be done so that L and M meet the calculated values. This can be done by measuring two inductance values. The first one is measured between terminal 3 and shorted terminals 1 and 2 and, as can be shown using model of Fig. 4, is equal ½·L. The second one is measured between terminals 1 and 3 with terminal 2 opened and is equal L + M.

Experimental results

Using the above procedure a coupled-inductor for the

1900 W telecom rectifier has been designed. The final results are: core E 55/28/25 - N27 (with $A_c = 4.2 \, cm^2$ and $A_w = 3.7 \, cm^2$), $N = 20$ turns, $l_{gc} = 5.3$ mm and $l_{go} = 0.3$ mm.

Such inductor was implemented in the rectifier and the experimental current waveforms in the transformer secondary and both inductor windings are presented in Figs. 16 a and b, respectively.
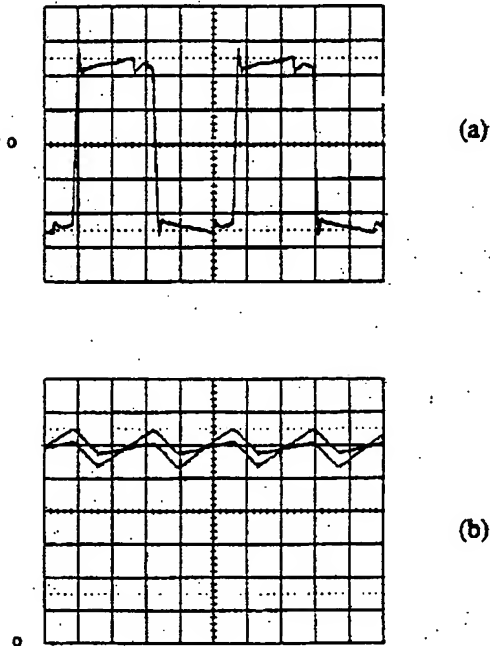

(a)

(b)

Fig. 16. Experimental current waveforms in the coupled-inductor current-doubler: (a) secondary transformer winding 5A/div, 2µs/div; (b) inductor windings: 2A/div.

7. CONCLUSIONS

In the paper the coupled-inductor version of the current-doubler topology was proposed and analysed. The analysis of the influence of the inductor coupling coefficient on the current and flux waveforms leads to the following conclusions.

1. The ac current waveforms in the coupled-inductor windings depend on the coupling coefficient k. With increasing value of k their amplitudes decrease and for k =1 reach minimum value.

2. The rms current values and thus power losses in both transformer and coupled-inductor windings decrease with increasing coupling coefficient k.

3. The sum of the two winding currents of the coupled-inductor (which equals the output current i_o) does not depend on the coupling coefficient k.

4. The ac flux waveforms in the coupled-inductor core do not depend on the coupling coefficient k.

5. The critical for core saturation flux value occurs in one of the outer legs of the coupled-inductor.

Summarising, the coupling of inductors in the current-doubler topology is recommended to reduce power losses in the secondary transformer and inductor windings. This can be achieved by integration of both inductors on a common core and by proper adjustment of the air-gaps.

REFERENCES

[1] C. Peng, M. Hannigan, O. Seiersen, "A new efficient high frequency rectifier circuit", Proc. of HFPC' 91, pp. 236-243.

[2] K. O'Meara, "A new output rectifier configuration optimized for high frequency operation", Proc. of HFPC' 91, pp. 219-226.

[3] L. Balogh, "Design review: 100W, 400kHz, dc/dc converter with current doubler synchronous rectification achieves 92% efficiency", Unitrode Seminar Manual 1996, pp. 2.1-2.25.

[4] N. Kutkut, "A full-bridge soft-switched telecom power supply with a current-doubler rectifier", Proc. of Intelec' 97, pp. 344-351.

[5] R. Redl, N. Sokal, L. Balogh, "A novel soft-switching full-bridge dc/dc converter: analysis, design considerations and experimental results at 1.5kW, 100kHz", PESC' 90 Record, pp. 162-172.

APPENDIX

To avoid core saturation the following condition must be observed:

$$\Phi_{1_{max}} = B_{sat} \cdot A_o \qquad (A1)$$

where A_o is the cross-section of the outer leg. Combining (6a) and (29) the following expression is obtained:

$$L = \frac{N \cdot A_o \cdot B_{sat}}{I_o \cdot (1 + \frac{2}{1-k} \cdot \frac{\Delta I}{I_o} + \frac{2-D}{2 \cdot (1-D)} \cdot \frac{\Delta i_o}{I_o})} \qquad (A2)$$

Assuming now that the dc winding losses are dominant the number of turns N can be expressed as:

$$N = \frac{A_w \cdot J_{30} \cdot K_{Cu}}{0.5 \cdot I_o} \qquad (A3)$$

where A_w is the core window area, K_{Cu} is the copper filling factor and J_{30} is the current density that would produce 30 deg. C inductor temperature rise with natural cooling. This value is empirically related to the core Area Product AP by:

$$J_{30} = 420 \cdot AP^{-0.24} \qquad (A/cm^2) \qquad (A4)$$

Inserting (A4) into (A3) and then result into (A2) and solving for $AP = A_w \cdot A_c$ gives finally eq. (31).

OFFICIAL PROCEEDINGS
OF THE THIRTEENTH
INTERNATIONAL

HFPC '98
(High Frequency Power Conversion)

Presented at

POWERSYSTEMS WORLD° '98
CONFERENCE & EXHIBIT

NOVEMBER 7 – 13, 1998
SANTA CLARA, CALIFORNIA

OFFICIAL PROCEEDINGS
OF THE THIRTEENTH
INTERNATIONAL

HFPC '98

(High Frequency Power Conversion)

Presented at

POWERSYSTEMS WORLD® '98
CONFERENCE & EXHIBIT

NOVEMBER 7 – 13, 1998
SANTA CLARA, CALIFORNIA

This Book Is the Property of:

_____

Conference Director
Myron A. Miller

Thirteenth International
HFPC (High Frequency Power Conversion) Conference
November 1998